HAL
open science

VLBA SiO observations of bright O-rich AGB stars

William D. Cotton, Guy Perrin, Bruno Lopez

To cite this version:

William D. Cotton, Guy Perrin, Bruno Lopez. VLBA SiO observations of bright O-rich AGB stars. Astronomy and Astrophysics - A&A, 2008, 477, pp.853-863. 10.1051/0004-6361:20077817 . hal-03785615

HAL Id: hal-03785615

https://hal.science/hal-03785615v1

Submitted on 6 Oct 2022

HAL is a multi-disciplinary open access archive for the deposit and dissemination of scientific research documents, whether they are published or not. The documents may come from teaching and research institutions in France or abroad, or from public or private research centers.

L'archive ouverte pluridisciplinaire **HAL**, est destinée au dépôt et à la diffusion de documents scientifiques de niveau recherche, publiés ou non, émanant des établissements d'enseignement et de recherche français ou étrangers, des laboratoires publics ou privés.

A&A 477, 853–863 (2008)
DOI: 10.1051/0004-6361:20077817
© ESO 2008

Astronomy & Astrophysics

VLBA SiO observations of bright O-rich AGB stars

W. D. Cotton[1], G. Perrin[2], and B. Lopez[3]

[1] National Radio Astronomy Observatory*, 520 Edgemont Road, Charlottesville, VA 22903-2475, USA
e-mail: bcotton@nrao.edu
[2] Observatoire de Paris, LESIA, UMR 8109, 92190 Meudon, France
[3] Observatoire de la Côte d'Azur, Nice, France

Received 8 May 2007 / Accepted 22 October 2007

ABSTRACT

We present the results of observations of the SiO masers at 7 mm wavelength in several oxygen rich Asymptotic Giant Branch (AGB) stars. These observations were coordinated with observations using the ESO VLTI/MIDI interferometer at 10 μm wavelength. These stars are *o* Ceti (Mira), U Herculis (U Her), OH26.5+0.6, R Leonis (R Leo), and W Hydrae (W Hya). Both total intensity and linear polarizations are imaged. Linear radial features seen in *o* Ceti may be associated with an X-ray flare seen a year earlier by Karovska et al. (2005). Similar linear features are also seen in R Leo, U Her and OH26.5+0.6. These features typically show systematic radial velocity variations and a tendency for the linear polarization to be perpendicular to the direction of elongation, suggesting that magnetic fields are dynamically important. A wide radial extent of the maser rings observed in U Herculis and OH26.5+0.6 is interpreted as meaning that the outer boundaries of the masing regions in these stars are not truncated by the condensation of SiO onto dust grains.

Key words. stars: atmospheres – stars: AGB and post-AGB – stars: variables: general – radio lines: stars – masers

1. Introduction

Asymptotic Giant Branch (AGB) stars are stars of a few solar masses and have reached the end of their lives; the inner core of the star has collapsed and the outer envelope has become very extended and is in the process of losing its mass to the interstellar medium through pulsational instabilities. In the cool, extended envelopes of these stars, molecules form and condense into dust. In oxygen rich stars, molecular masers appear, especially SiO, H_2O and OH at respectively increasing distance from the photosphere (Reid & Moran 1981). The SiO masers occur within a few stellar radii of the stellar surface between the hot molecular inner envelope and the cooler region at 3−5 $R_\star$ where the (silicate) dust forms; see Reid & Menten (1997), Danchi et al. (1994). The detailed mechanics driving mass loss is not well understood; nor is the reason that many planetary nebulae are very asymmetric whereas their AGB progenitors appear circularly symmetric.

Circumstellar SiO masers tend to occur in clumpy, partial rings centered on the central star (Diamond et al. 1994). A long path through relatively constant (radial) velocity gas is needed for the masers to develop the necessary gain to be visible. This condition is most often met for lines of sight tangent to the masing layer in regions of relatively low turbulence. Turbulence will reduce the path length at a given velocity limiting the gain, hence brightness, of the corresponding maser spot. The resulting maser spots tend to appear in a partial ring. Thus, these masers become markers for the layer in which the physical conditions necessary for the masers exist and tracers of the dynamics of these regions. Humphreys et al. (1996) and Humphreys et al. (2002) discuss the dynamics of circumstellar SiO masers.

High resolution observations of the SiO masers in this dynamically significant region provide a powerful probe. The frequent monitoring of the SiO masers in TX Cam by Diamond & Kemball (2003) show complex motions of the masing gas; both outward and inward motions are detected.

The polarization of circumstellar masers is a valuable probe of magnetic fields in circumstellar envelopes. The complex theory of maser polarization, and particularly that of the SiO masers, is described in a number of publications (e.g. Deguchi & Watson 1990; Nedoluha & Watson 1990; Elitzur 1991; Nedoluha & Watson 1994; Elitzur 1996). Observations of TX Cam by Kemball & Diamond (1997) revealed tangentially ordered polarization vectors indicating a radial magnetic field direction and circular polarization indicating a magnetic field strength of several Gauss. Cotton et al. (2006) also found some evidence for ordered fields in a number of stars as well as evidence of a significant dynamical role of magnetic fields in a number of stellar SiO masers. The influence of magnetic fields is illustrated by the recent detection of a magnetically collimated jet around an evolved star (Vlemmings et al. 2006).

One of the difficulties in understanding these stars is that of determining the apparent photospheric size. Ireland et al. (2004) have used the aperture masking interferometry technique to measure the sizes of a number of AGB stars in the red through near IR. The sizes of AGB stars all increase systematically towards the blue and were larger than expected at all wavelengths. The authors speculated that this was due to scattering by dust in the inner envelope. Ireland & Scholz (2006) calculate various models of dust formation and conclude that for a number of cases, the inner diameter of the dust shell would be 2−3 times that of the photosphere. Monnier et al. (2004) used a combination of aperture masking on Keck with interferometric measurements using IOTA at 2.2 μm to image a number of stars with dust shells. They

* The National Radio Astronomy Observatory (NRAO) is operated by Associated Universities Inc., under cooperative agreement with the National Science Foundation.

Article published by EDP Sciences and available at http://www.aanda.org or http://dx.doi.org/10.1051/0004-6361:20077817

determined that the shells in a number of stars, including Miras were clumped.

Perrin et al. (2004) observed a number of Mira variables between 2.2 and 3.6 μm and derived large variations of the apparent size with wavelength. They interpreted the variation in size as being due to a molecular shell containing H_2O and a wavelength dependent opacity.

Ohnaka et al. (2005) observed the Mira variable RR Sco at 2.2 and 10 μm using the VLTI and modeled the star with a photosphere surrounded by an optically thick envelope of H_2O and SiO 2.3 times the photospheric size and surrounded by an optically thin dust shell with an inner diameter of 7−8 times the photospheric size. 11 μm observations of Danchi et al. (1994) also found considerable variations in the ratio of the size of the inner dust shell to the size of the photosphere. However, Cotton et al. (2004) found a fairly small scatter of the ratio of the SiO maser ring diameter to the apparent size at 2.2 μm around a value of approximately 2. The relation of the SiO maser ring diameter to the inner size of the dust shell is unclear.

In this paper we report the VLBA observational part of a coordinated set of observations using the VLBA and the ESO VLTI/MIDI interferometers. The VLTI/MIDI instrument works in the mid infrared at around 10 μm and is very sensitive to the region of dust formation. The SiO maser observations serve as a probe of the physical conditions and dynamics of the stellar envelope just interior to the region of dust formation. Initial VLTI/MIDI results are given in Menut et al. (2004), Chesneau et al. (2005) and Ohnaka et al. (2005). Further VLTI/MIDI results and a joint interpretation will be reported in subsequent publications.

2. Observations and data reduction

The new observations were obtained with the NRAO Very Long Baseline Array (VLBA) during a 20 h session on 5 September 2004. Two 4 MHz wide channels in each right- and left-hand circular polarization were recorded at 42.820587 and 43.122027 GHz to cover the $\nu = 2$, $J = 1{-}0$ and $\nu = 1$, $J = 1{-}0$ transitions of SiO. Two bit sampling was used in the recording. The correlations resulted in 128 channels in each of the combinations of right- and left-circular polarization for each transition. A strong, nearby continuum source was observed before each star to serve as delay, bandpass and polarization calibrator. The observations are summarized in Table 1 which lists the stars, calibrators, and central velocities. The calibrators are all quasars with milliarcsecond accuracy positions; the Hipparcos (ESA 1997) positions of the stars (except OH26.5+0.6), evaluated at the epoch of the observations, were used. Note: the center velocities were picked to center the spectra in the observing band and are not necessarily the stellar systemic velocities.

Calibration and processing follows the procedure described in Cotton et al. (2004) and Cotton et al. (2006) except as noted below. Calibration was done in the NRAO AIPS package and imaging and subsequent processing in the Obit package (`http://www.cv.nrao.edu/~bcotton/Obit.html`). Linear polarization calibration was based on monitoring of the continuum calibrators from the VLA and, in general, the calibration of polarization angle should be better than 10 degrees. An error in the calibration of the polarization angle will be common to all images shown here. Velocity images are derived from a flux density weighted average velocity of pixels with significant emission.

Table 1. AGB stars observed.

Star	Calibrator	Vel A[1] (km s^{-1})	Vel B[2] (km s^{-1})	Distance[3] pc	Phase[4]
o Ceti	J0217+0144	48.0	45.0	128 ± 18	0.35
R Leonis	J0854+2006	2.0	–1.0	101 ± 20	0.00
W Hydrae	J1337-1257	41.7	41.7	115 ± 14	0.65
U Herculis	J1613+3412	–14.0	–16.0	610 ± 490	0.34
OH26.5+0.6	J1751+0939	29.0	29.0		0.34

[1] $\nu = 2$, $J = 1{-}0$ transition of SiO at 42.8 GHz; [2] $\nu = 1$, $J = 1{-}0$ transition of SiO at 43.1 GHz; [3] Distance from Hipparcos (ESA 1997) parallax; [4] Pulsation phase.

3. Results

The integrated total intensity and velocity images for each transition with superposed polarization "E" vectors are shown in Figs. 1−5.

3.1. Ring diameter

The diameters and widths of the SiO maser rings were determined from a moment analysis of compressed (2D) Stokes *I* images in both transitions using a direct parameter search which minimized the sum of the ring widths. The independent ring diameters and widths were determined jointly for the two transitions but with a common center. This procedure, especially the estimated ring widths may be adversely affected by residual errors in the alignment of the images in the two transitions. The distribution of emission in OH26.5+0.6 was sufficiently asymmetric that the center was not well fitted so this was estimated "by eye". The fitted ring diameters and width for each star and transition are shown in Table 2.

3.2. Polarization

The vectors in Figs. 1–5 are proportional to the linearly polarized intensity, and their orientation defines the plane of the electric field. The relationship between the orientation of linear polarization and the magnetic field is relatively complex (see discussion in Cotton et al. (2006)) but under many circumstances, the emitted linear polarization is perpendicular to the magnetic field.

The magnetic field strength can be measured directly from Zeeman splitting of the maser lines in Stokes *V* measurements. Unfortunately, processing the data from these observations pushed the limits of the capacity of the VLBA correlator and it was not possible to obtain sufficient spectral resolution to make meaningful measurements of the Zeeman splitting.

3.3. o Ceti

The images of the masers in *o* Ceti seen in Fig. 1 show an irregular shape approximately 74 mas in diameter at pulsation phase 0.35. This is consistent with results from several epochs reported by Cotton et al. (2004) and Cotton et al. (2006). Only portions of a ring structure are seen. The polarized regions shown in Fig. 1 are largely associated with linear, radial features and the polarization is generally perpendicular to the features suggesting a parallel magnetic field.

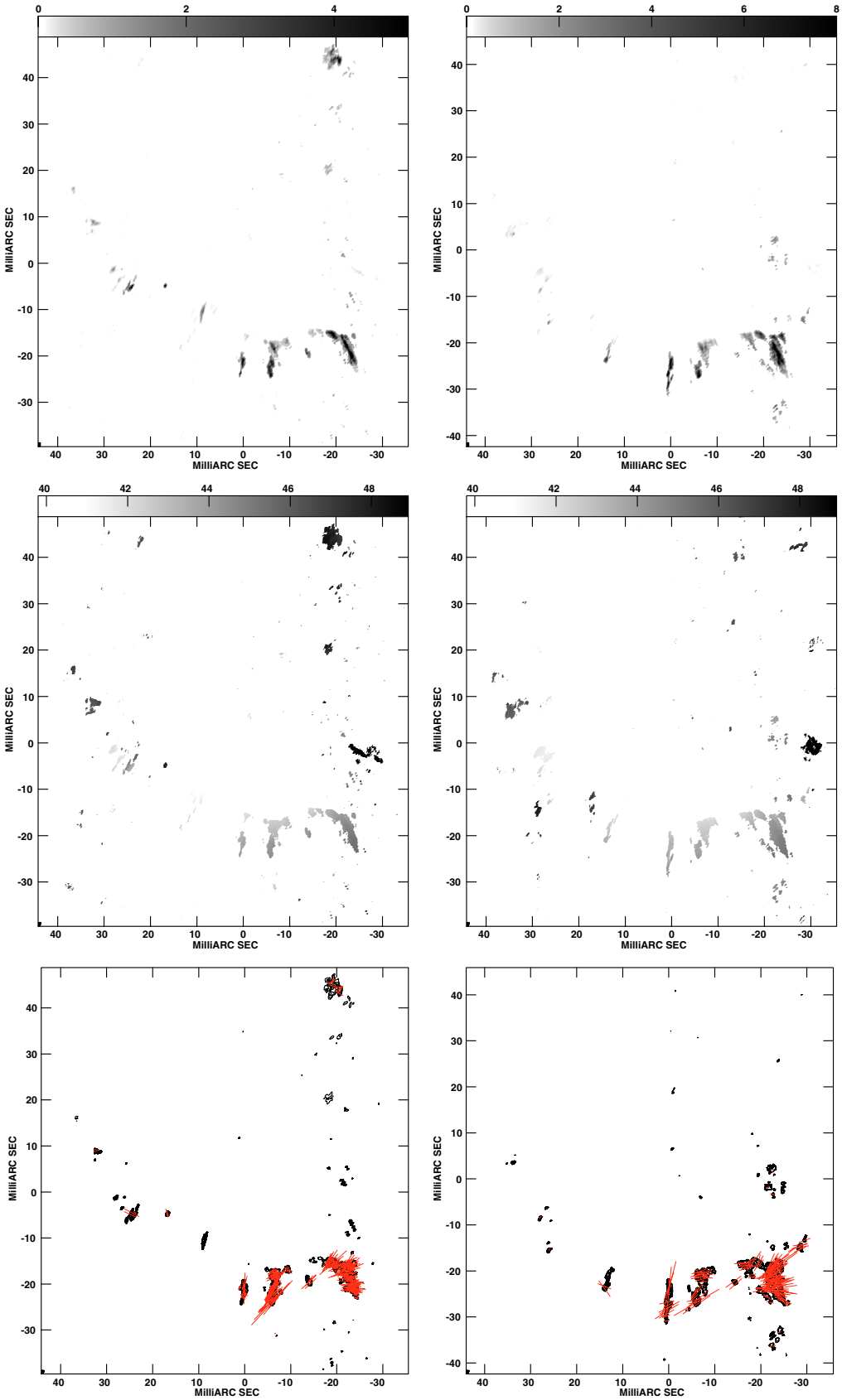

Fig. 1. *o* Ceti (Mira). *The left column* is the $v = 2$, $J = 1{-}0$ transition of SiO at 42.8 GHz, *the right column* is the $v = 1$, $J = 1{-}0$ transition of SiO at 43.1 GHz. *The top plots* are the total intensity as a reversed gray-scale, *the middle plots* are velocity averages of pixels with significant emission, and *the bottom plots* are total intensity contours (spaced by powers of two) with polarization "E" vectors over-plotted in red.

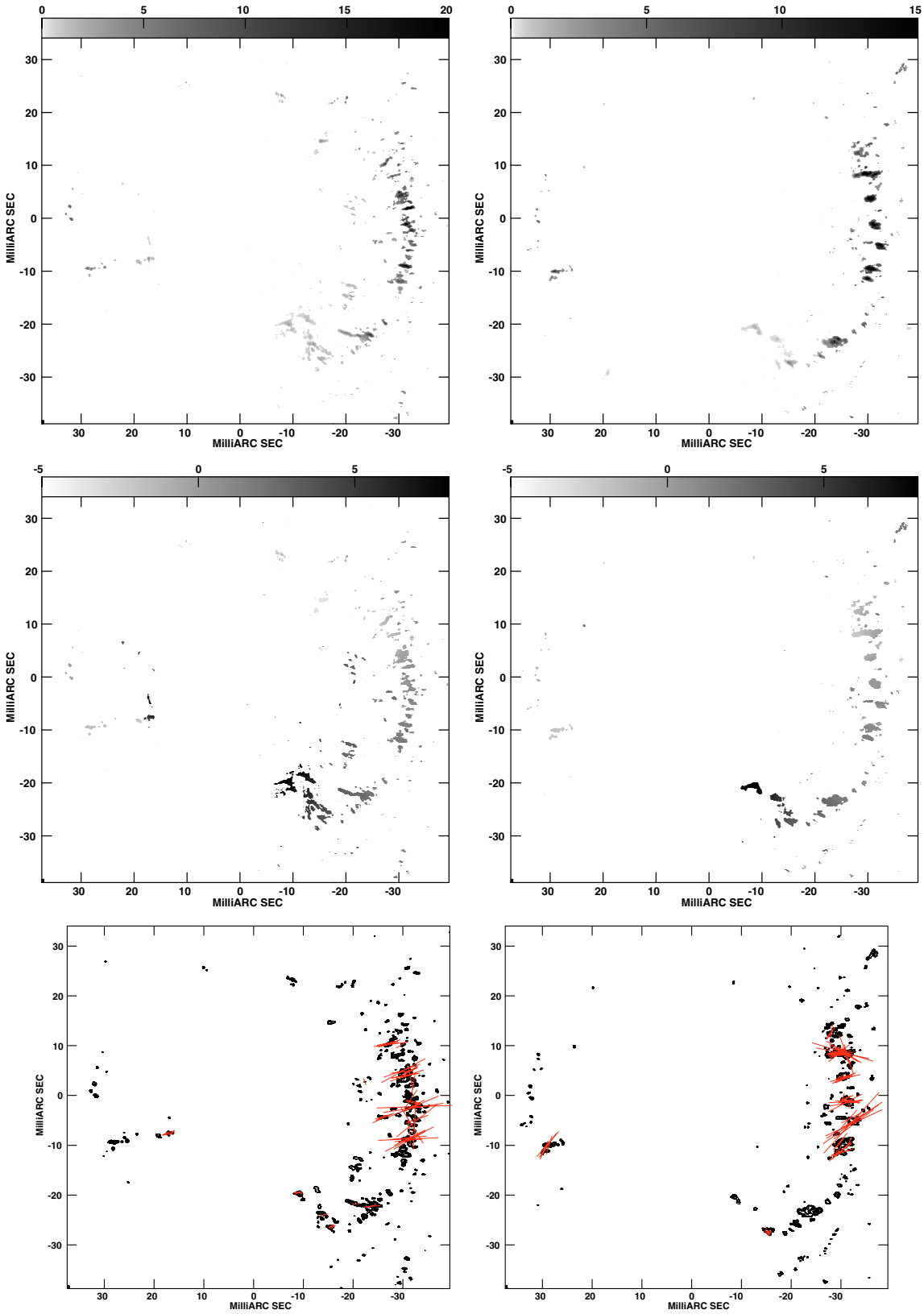

Fig. 2. R Leonis. *The left column* is the $v = 2$, $J = 1{-}0$ transition of SiO at 42.8 GHz, *the right column* is the $v = 1$, $J = 1{-}0$ transition of SiO at 43.1 GHz. *The top plots* are the total intensity as a reversed gray-scale, *the middle plots* are velocity averages of pixels with significant emission, and *the bottom plots* are total intensity contours (spaced by powers of two) with polarization "E" vectors over-plotted in red.

3.4. R Leonis

The masers in R Leonis seen in Fig. 2 show a partial ring approximately 62 mas in diameter at pulsation phase 0.00. This is consistent with previous results over a range of phase. Cotton et al. (2004) also show partial rings, but mostly on the northern and eastern sides whereas in Fig. 2 a well developed structure

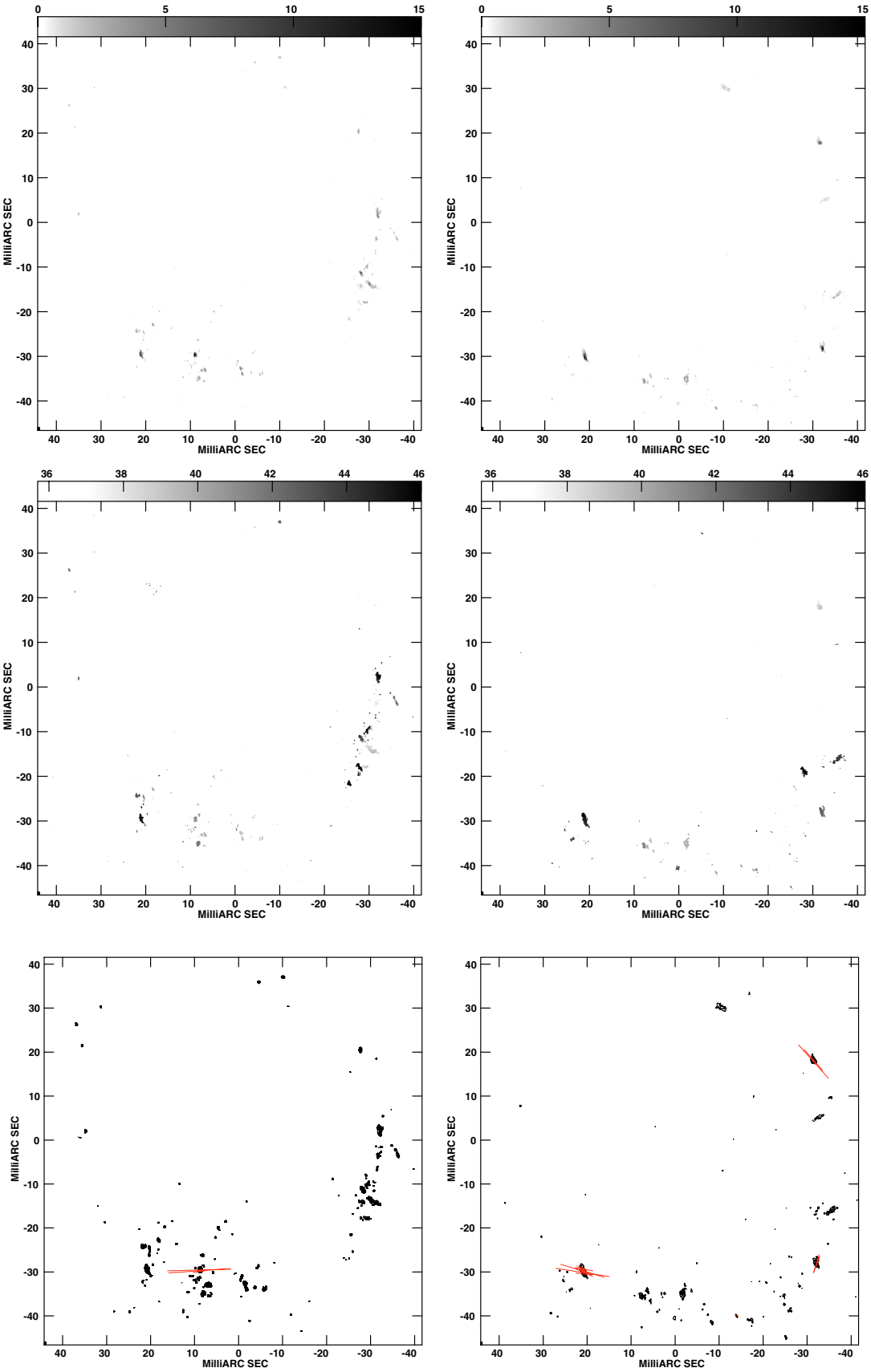

Fig. 3. W Hydrae. *The left column* is the $v = 2$, $J = 1{-}0$ transition of SiO at 42.8 GHz, *the right column* is the $v = 1$, $J = 1{-}0$ transition of SiO at 43.1 GHz. *The top plots* are the total intensity as a reversed gray-scale, *the middle plots* are velocity averages of pixels with significant emission, and *the bottom plots* are total intensity contours (spaced by powers of two) with polarization "E" vectors over-plotted in red.

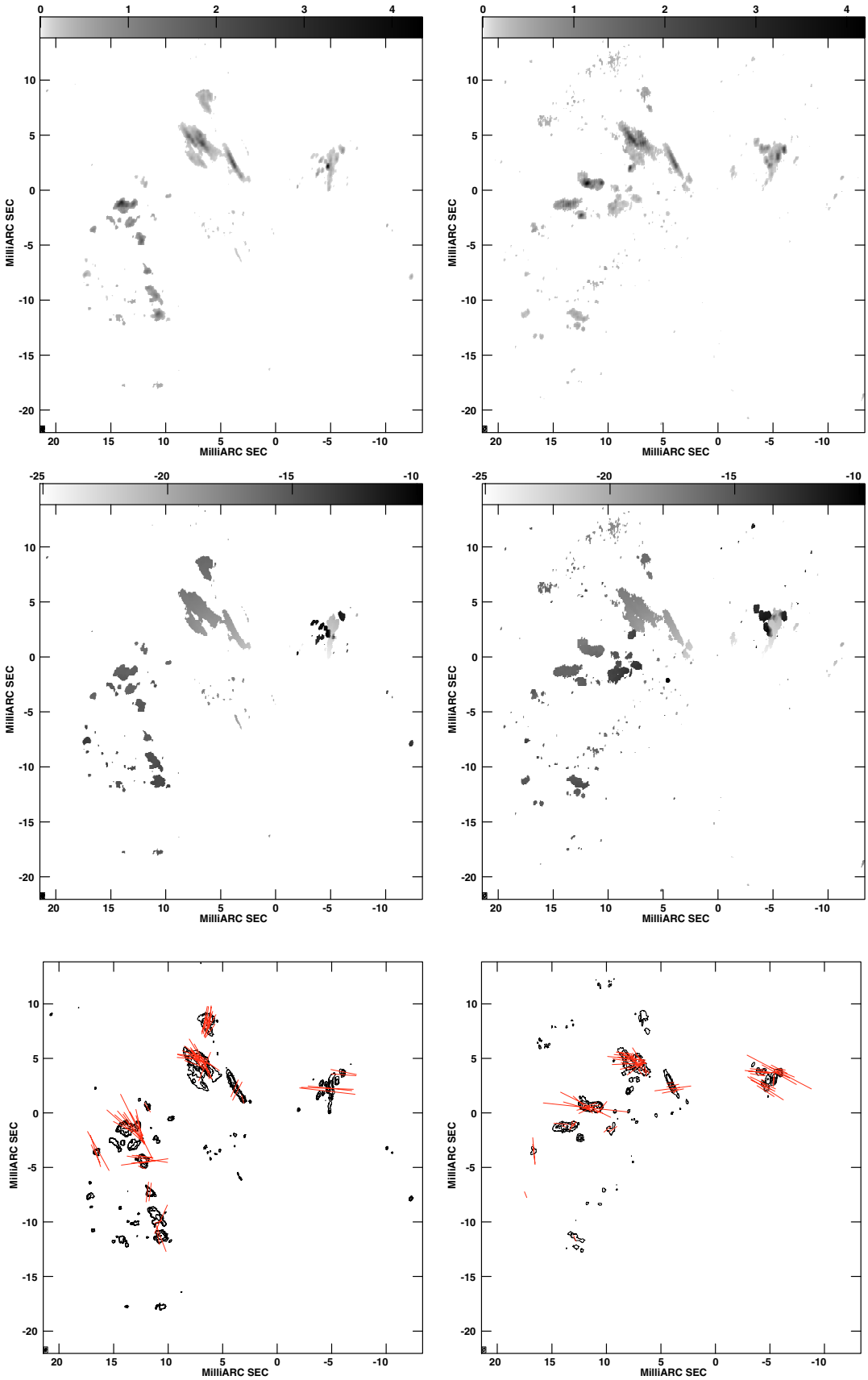

Fig. 4. U Herculis. *The left column* is the $v = 2$, $J = 1{-}0$ transition of SiO at 42.8 GHz, *the right column* is the $v = 1$, $J = 1{-}0$ transition of SiO at 43.1 GHz. *The top plots* are the total intensity as a reversed gray-scale, *the middle plots* are velocity averages of pixels with significant emission, and *the bottom plots* are total intensity contours (spaced by powers of two) with polarization "E" vectors over-plotted in red.

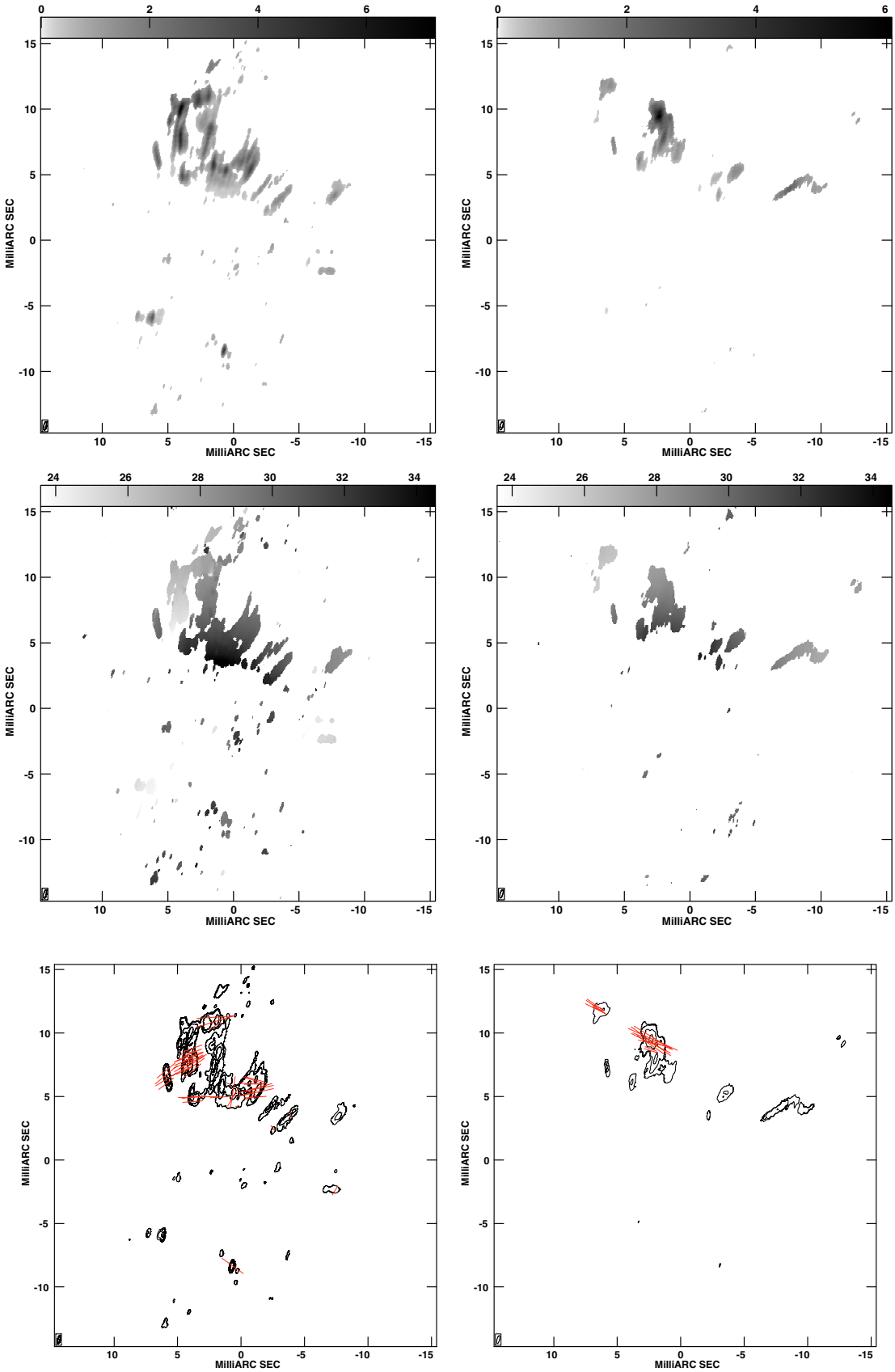

Fig. 5. OH26.5+0.6. *The left column* is the $v = 2$, $J = 1{-}0$ transition of SiO at 42.8 GHz, *the right column* is the $v = 1$, $J = 1{-}0$ transition of SiO at 43.1 GHz. *The top plots* are the total intensity as a reversed gray-scale, *the middle plots* are velocity averages of pixels with significant emission, and *the bottom plots* are total intensity contours (spaced by powers of two) with polarization "E" vectors over-plotted.

Table 2. SiO ring diameters.

Source	$\nu = 1^1$ diam (mas)	width	$\nu = 2^2$ diam (mas)	width	$\nu = 1$ diam (AU)	width	$\nu = 2$ diam (AU)	width
o Ceti	71.1	2.6	68.6	2.3	9.1	0.3	8.8	0.3
R Leonis	62.1	0.7	62.6	0.6	6.3	0.07	6.3	0.06
W Hydrae	72.0	1.3	60.0	3.2	8.3	0.15	6.9	0.4
U Herculis	22.9	1.1	22.0	1.4	14.0	0.7	13.4	0.9
OH26.5+0.6[3]	22.1	0.3	19.4	2.2				

Notes: [1] $\nu = 1$, $J = 1{-}0$ transition of SiO at 43.1 GHz; [2] $\nu = 2$, $J = 1{-}0$ transition of SiO at 42.8 GHz; [3] Center not fitted, no parallax available.

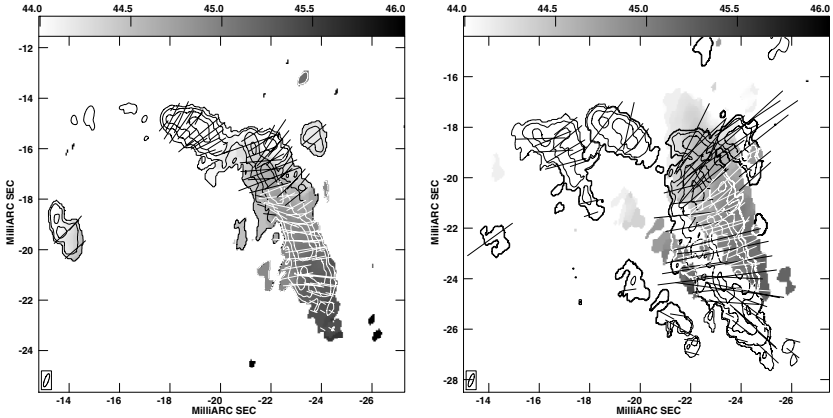

Fig. 6. *o* Ceti. Closeup of a region in Fig. 1. *Left* is the $\nu = 2$, $J = 1{-}0$ transition of SiO at 42.8 GHz, on *the right* is the $\nu = 1$, $J = 1{-}0$ transition of SiO at 43.1 GHz. The gray scale is the average velocity as given by the scale-bar at the top of each plot, contours are total intensity with an interval of powers of two, and polarization "E" vectors are over-plotted. The center of the star is to the upper left. The resolution is shown in a box in the lower left corner.

is seen on the western side. The maser ring appears larger than was typical in the 2001 observations of Cotton et al. (2004). The polarization vectors shown in Fig. 2 are largely perpendicular to the ring suggesting a tangential field.

3.5. W Hydrae

The masers in W Hydrae (Fig. 3) form a symmetric partial ring to the south and west with a diameter of ~70 mas at pulsation phase 0.65. This is substantially smaller than the ~80 mas diameter reported by Cotton et al. (2004) (phase 0.53). Only a few of the maser spots show significant linear polarization although the polarization angle is generally tangent to the ring suggesting a radial nature of the magnetic field.

3.6. U Herculis

The masers in U Herculis shown in Fig. 4 exhibit an irregular shape approximately 20 mas in size at pulsation phase 0.34. This is somewhat smaller that the typical size, ~25 mas, at multiple epochs in 2001 reported by Cotton et al. (2004) and with a shape far more irregular than the 2001 results. The polarization vectors shown in Fig. 4 are relatively chaotic although with a tendency to be orthogonal to linear features.

3.7. OH26.5+0.6

The masers in OH26.5+0.6 (see Fig. 5) largely consist of plumes to the north of a ring with a diameter of 13.7 mas defined by several bright spots. The polarized regions in Fig. 5 are mostly associated with the plumes to the north and show a weak tendency for the orientation to be orthogonal to structures.

4. Jet-like features

In a number of the maser images presented here and in Cotton et al. (2006) there are extended, linear features aligned with the direction to the photosphere. These frequently have similar morphologies in both the transitions observed with similar runs of velocity which vary systematically along their lengths. Since these features are near the masing ring, these velocities will be predominantly non-radial with respect to the star so do not represent simple acceleration of the masing material away from the star. The apparent alignment of the magnetic field with these features could be due either to the magnetic field being stretched along the features by the ionized component of the gas or the gas being constrained by its ionized component to move along field lines, depending on the relative energy density of the magnetic field. SiO maser observations (Herpin et al. 2003, 2006) and H_2O maser observations (Vlemmings et al. 2005, 2006) suggest that magnetic fields are likely dynamically important in which case the maser jet-like features are following the magnetic field.

4.1. o Ceti

Jet-like features in *o* Ceti have previously been discussed by Cotton et al. (2006) in which the radial velocities were furthest from systemic closest to the star and the polarization "E" vectors perpendicular to the feature. A close up view of the linear features in Fig. 1 is given in Fig. 6. These features are at a very different orientation than the 2001 features but also show radial velocities which are furthest from systemic closest to the star and the polarization "E" vectors perpendicular to the features.

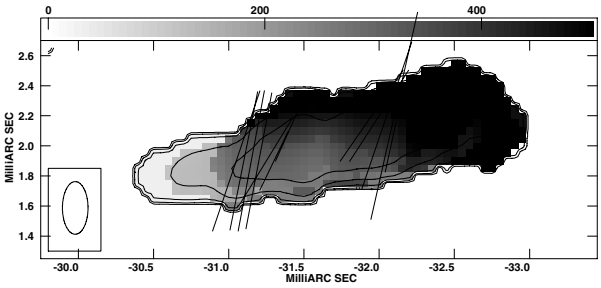

Fig. 7. R Leonis. Closeup of a region in Fig. 2 in the $v = 2$, $J = 1-0$ transition of SiO at 42.8 GHz. The gray scale is the average velocity as given by the scale-bar at the top, contours are total intensity with an interval of powers of two, and polarization "E" vectors are over-plotted. The center of the star is to the left. The resolution is shown in a box in the lower left corner.

4.2. R Leonis

Figure 2 shows a number of linear features to the west of the star; the most prominent of these is shown in more detail in Fig. 7. In this case, the velocities closest to the star are closest to systemic. While the polarization from this feature is weak, the polarization vectors are more nearly perpendicular than parallel.

4.3. U Herculis

One of the more prominent regions of plumes to the north seen in Fig. 4 is shown in detail in Fig. 8. In this case the regions closest to the star are further from systemic than more distant regions. The linear polarization along the features shown in Fig. 8 show a mixture of orientation to the direction of the feature, parallel, perpendicular and oblique angles are seen. The narrowest feature has polarization "E" vectors perpendicular to the direction.

4.4. OH26.5+0.6

Details of the regions of maser plumes to the north in Fig. 5 are shown in Fig. 9. The velocities in these features show a complex pattern including the entire range of velocities seen in this star. The linear polarization in the better defined linear features is perpendicular to the feature.

5. Discussion

The general picture of the atmospheres of O-rich AGB stars is that the SiO maser appear just interior to the region in which the dust forms. Since the dust cannot condense until the gas temperature drops below the condensation temperature, the dust will form a shell around the star. A comparison of measured or modeled inner diameters of the circumstellar dust shells can test this picture. Previous IR measurements and the mean values from Table 2 are shown in Table 3. Note, the 2.2 μm diameters include contributions from the molecular layer and are larger than the photosphere.

5.1. o Ceti

An X-ray outburst was reported in Mira A (the AGB component) on 6 Dec. 2003 by Karovska et al. (2005). It was postulated that this event was associated with a large mass ejection event and a dust ejection was predicted.

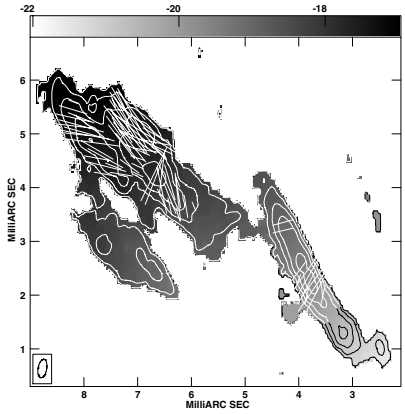

Fig. 8. U Herculis. Closeup of a region in Fig. 4 in the $v = 2$, $J = 1-0$ transition of SiO at 42.8 GHz,. The gray scale is the average velocity as given by the scale-bar at the top, contours are total intensity with an interval of powers of two, and polarization "E" vectors are over-plotted. The star center is to the lower right. The resolution is shown in a box in the lower left corner.

Table 3. IR diameters.

Source	2.2 μm diam (mas)	Photo 11 μm diam (mas)	Dust 11 μm diam (mas)	SiO diam (mas)
o Ceti	28.8[1]	25.6[2]	50[3]	69.8
R Leonis	30.7[1]	26.3[3]	70[3]	62.3
W Hydrae	39.9[4]			66.0
U Herculis	11.0[1]			20.8
OH26.5+0.6[3]		~7[5]	~40[5]	20.8

Notes: [1] Mennesson et al. 2002; [2] Weiner (2004); [3] Danchi et al. (1994); [4] Millan-Gabet et al. (2005); [5] Model from Suh (2004).

Ireland et al. (2004) gives aperture masking results which show that the photosphere is not well modeled with a uniform disk and a Gaussian model is used instead. The size of the Gaussian FWHM varied systematically from about 40 mas at 0.68 μm to 20 mas at 0.92 μm with significantly larger sizes seen in the TiO bands (phase 0.34).

Interferometric measurements at 2.2 μm using the VLTI/VINCI instrument are reported by Woodruff et al. (2004) who show the diameter varying between 29 and 35 mas. Measurements using several narrow bands near 2.2 and 3.6 μm using the IOTA/FLUOR interferometer lead Perrin et al. (2004) to conclude that the star had a molecular layer in which opacity due to H_2O caused the apparent variation of size with wavelength. The photospheric diameter reported was 26.8 mas in 2000 (phase 0.01) and 25.0 mas in 2001 (phase 0.20).

Danchi et al. (1994) reports 11 μm observations to which a photospheric diameter varying between 38.6 and 47.2 mas and an inner diameter of the dust shell of 120 mas was fit. Subsequent measurements with the ISI at 11 μm by Weiner et al. (2003b) from 1999 to 2001 gave a diameter varying between 42.6 and 48 mas and some evidence for an asymmetric structure. Later, modeling by Weiner (2004) concluded that the 11 μm data could be explained by a photospheric diameter of 25.6 mas surrounded by a shell of H_2O with a diameter of 60.5 mas. Atmospheric modeling by Ohnaka et al. (2005) concluded that both interferometric and spectroscopic observations of *o* Ceti could largely be explained by an H_2O layer surrounding the star. Modeling of the SED of *o* Ceti was reported by Suh (2004) who claimed that a 10 μm opacity of only 0.01–0.02 could account for the observed SED. This modeling concluded that the inner diameter

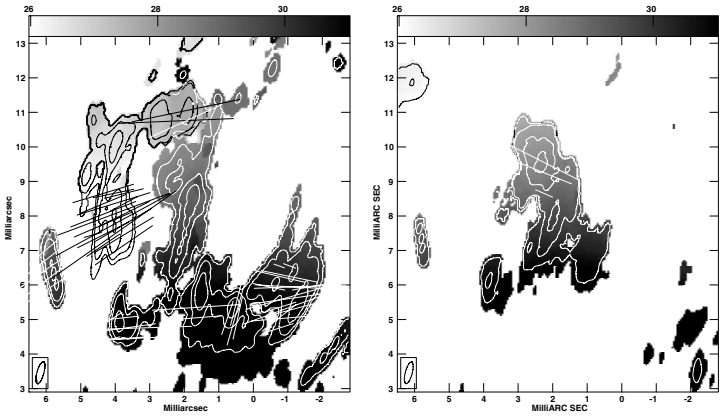

Fig. 9. OH26.5+0.6. Closeup of a region in Fig. 5. *Left* is the $v = 2$, $J = 1{-}0$ transition of SiO at 42.8 GHz, on *the right* is the $v = 1$, $J = 1{-}0$ transition of SiO at 43.1 GHz. The gray scale is the average velocity as given by the scale-bar at the top, contours are total intensity with an interval of powers of two, and polarization "E" vectors are over-plotted. The center of the star is below. The resolution is shown in a box in the lower left corner.

of the dust shell was 27 to 30 times the diameter of the star or considerably larger than observed by Danchi et al. (1994).

McIntosh (2006) reports on frequent spectroscopic monitoring of several of the SiO masers in *o* Ceti. The $v = 1$, $J = 1{-}0$ transition showed a correlation of velocity with integrated flux density over the pulsation cycle. Interferometric monitoring of SiO masers during 2001 are reported by Cotton et al. (2004); the ring diameter varied between 60 and 75 mas. Cotton et al. (2006) report observations at an additional four epochs in 2003 and 2004 with SiO maser ring diameters varying from 60 to 80 mas.

The diameter of the the SiO ring given in Table 2, 69.8 mas, is within the range previously reported by Cotton et al. (2004) and Cotton et al. (2006) and is somewhat larger than the 50 mas inner diameter of the dust shell reported by Danchi et al. (1994). This is consistent with the SiO masers marking the region just interior to the region of silicate dust formation.

Figures 1 and 6 show systematic velocity variations along numerous radial features. In these features, the observed radial velocities are furthest from systemic closest to the photosphere. Since the line of sight is tangent to the maser ring, these motions are tangential as seen by the star and so are not explained by simple radial accelerations. The predominantly perpendicular polarization vectors seen in Fig. 6 suggest that these motions are controlled by the magnetic field of the star.

It is possible that the radial features seen in Figs. 1 and 6 are the result of a mass ejection associated with the X-ray burst a year earlier reported by Karovska et al. (2005). At the Hipparcos (ESA 1997) distance of 128 pc, the average projected velocity of material ejected in the flare reaching the position of the linear feature seen in Fig. 6 is about 13 km s^{-1}. This value is somewhat larger than the total range of maser velocities observed in the star but higher than average velocities for ejected material closer to the stellar surface are likely.

Similar linear features were prominent during only one of the four epochs during 2001 sampled by Cotton et al. (2004). This leads to the possibility that stellar flaring activity may contribute to the overall mass loss process.

5.2. R Leonis

Masked aperture interferometry by Ireland et al. (2004) between 0.68 and 0.92 μm show an increasing size towards the blue going from 22 to 40 mas (phase 0.91). Non-zero closure phases indicate asymmetries in the structure. Monnier et al. (2004) used a combination of aperature masking on Keck with interferometric measurements using IOTA at 2.2 μm to image R Leo. A uniform disk of diameter 30.3 mas (phase 0.90) adequately explained the data. R Leo was observed by Fedele et al. (2005) at 2.2 μm using VLTI/VINCI who derived diameters of 28.5 and 26.2 mas at successive maxima. The shape of the visibility curve was consistent with a circumstellar molecular envelope. Millan-Gabet et al. (2005) give H and K band apparent sizes of 23.8 and 29.9 mas measured with IOTA (phase 0.4). Schuller et al. (2004) attempted modeling observations of R Leo and concluded that a model with only a photosphere and a dust shell could account for observations at 2.2 and 11 μm but not 3.6 μm. Using several narrow band observations between 2.2 and 3.6 μm, Perrin et al. (2004) fitted a model of a photospheric diameter of 21.8 mas surrounded by an H_2O layer 50 mas in diameter in 2000−2001.

Weiner et al. (2003a) report measurements on R Leo at 11 μm with ISI measured apparent sizes between 55.3 and 64.2 mas in the period 1999−2001. ISI observations at 11 μm by Tatebe et al. (2006) show dramatic changes in the star to dust ratio between 2003 and 2004 (less dust in 2004) but zero closure phases suggest symmetric structure.

Cotton et al. (2004) observed R Leo at four epochs during 2001 and reported variations of the SiO ring diameter of 50 to 61 mas. At none of these epochs was anything like the striking set of linear features shown in Figs. 2 and 7 seen. The diameter of the SiO ring given in Table 3, 62.3 mas is at the upper end of the range of values seen in 2001 and is slightly smaller than the inner diameter of the dust shell, 70 mas, from Danchi et al. (1994). This size is slightly larger that the estimated size of the molecular layer, 50 mas, estimated by Perrin et al. (2004) (phase 0.80).

5.3. W Hydrae

On the basis of modeling of ISO spectroscopy, Justtanont et al. (2004) argue for a warm CO_2 layer between the photosphere and the dust shell. Masked aperture interferometry by Ireland et al. (2004) between 0.68 and 0.92 μm show an increasing size towards the blue going from 40 to 70 mas (phase 0.44) with some evidence of asymmetric structure. Monnier et al. (2004) used a combination of aperture masking on Keck with interferometric measurements using IOTA at 2.2 μm to image W Hya. A uniform disk model (42.5 mas) gave a poor fit (phase 0.00).

Millan-Gabet et al. (2005) give H and K band apparent sizes of 32.2 and 39.9 mas measured with IOTA (phase 0.6).

Cotton et al. (2004) observed W Hya in August 2001 and give an average SiO ring diameter of 80 mas which as considerably larger than the 66 mas given in Table 3.

5.4. U Herculis

Ragland et al. (2006) fit a uniform disk model at H band with a diameter of 9.7 mas in Jun. 2002 using IOTA. A non-zero closure phase indicates asymmetric structure. Mennesson et al. (2002) give a uniform disk diameter of 11 mas at 2.2 μm and 14.3 mas at 3.6 μm in 2000 (phase 0.25). U Her was observed at four epochs in 2001 by Cotton et al. (2004) and had a maser ring diameter between 22 and 25 mas. The ring diameter given in Table 3 of 22.8 mas is within this range.

The character of the source is quite different as shown in Figs. 4 and 8 and in the 2001 images of Cotton et al. (2004); showing more extended emission and a more chaotic and less ring-like structure in the observations presented here. This is illustrated in the ring widths in Table 2 which are roughly twice the typical value in Cotton et al. (2004). Figure 8 shows linear radial features with systematic radial velocity variations; this type of feature was not observed during 2001. The large radial extent of the masing region suggests that its outer size in not being truncated by condensation of SiO onto grains.

5.5. OH26.5+0.6

Chesneau et al. (2005) reports on the MIDI observations of OH26.5+0.6. The star was resolved by the beams of the 8 m telescopes with a strong asymmetry and a size of 286 × 214 mas. No fringes were detected interferometrically. However, modeling of the SED by Suh (2004) predicts an opacity between 15 and 22 at 10 μm which would obscure the central star. The lack of interferometric detection of the dust shell suggests that it is quite smooth. The modeling of Suh (2004) predicts that the inner diameter of the dust shell will be approximately 40 mas, or roughly twice the diameter of the SiO maser ring from Table 3. The image of the SiO masers shown in Figs. 5 and 9 show a relatively chaotic structure with a very large width. This is consistent with the prediction of Suh (2004) that the maser ring is well inside the dust condensation radius and that the masers are not truncated on the outer edge by the SiO condensing onto grains.

6. Conclusions

We present new total intensity and linear polarization VLBA observations of the $\nu = 2$ and $\nu = 1$ $J = 1{-}0$ maser transitions of SiO at 42.8 and 43.1 GHz of a number of AGB stars being studied jointly with the VLBA and VLTI/MIDI interferometers.

The unusually large radial extent of masers around U Herculis and OH26.5+0.6 suggest that the outer regions of the maser ring are not being truncated by the condensation of the SiO onto dust grains. In the latter case, this is supported by the modeling of Suh (2004) suggesting that the region of dust condensation is well outside of the region in which masers are observed. If this conjecture is correct, then the stellar distance of dust formation is variable in U Herculis as earlier observations by Cotton et al. (2004) show a much narrower radial extent of the SiO masing region. These observations support the suggestion that the physical conditions in the outer envelopes of these stars are quite variable in time.

There is an intriguing possibility of an association of the X-ray flare in Mira reported by Karovska et al. (2005) with the linear features seen in the SiO maser images presented here. This suggests that flaring activity could play a role in the mass-loss process.

The polarization structure of the linear features also show a preference for the E vectors to be perpendicular to the direction of the feature; this is interpreted as indicating magnetic fields oriented primarily along the feature. Two possible explanations for this are the magnetic field being dragged by the ionized component of the envelope or the magnetic field controlling the motion of the accelerating material. Several recent SiO and H_2O maser observation indicate that the magnetic field will be dynamically important (Herpin et al. 2003; Vlemmings et al. 2005, 2006). Thus, the jet-like structure are likely due to the masing regions being dragged along the magnetic field. Observations of such features sufficiently closely spaced in time to measure proper motions should help understand the nature of these features.

References

Chesneau, O., Verhoelst, T., Lopez, B., et al. 2005, A&A, 435, 563
Cotton, W. D., Mennesson, B., Diamond, P. J., et al. 2004, A&A, 414, 275
Cotton, W. D., Vlemmings, W., Mennesson, B., et al. 2006, A&A, 456, 339
Danchi, W. C., Bester, M., Degiacomi, C. G., Greenhill, L. J., & Townes, C. H. 1994, AJ, 107, 1469
Deguchi, S., & Watson, W. D. 1990, ApJ, 354, 649
Diamond, P. J., & Kemball, A. J. 2003, ApJ, 599, 1372
Diamond, P. J., Kemball, A. J., Junor, W., et al. 1994, ApJ, 430, L61
Elitzur, M. 1991, ApJ, 370, 407
Elitzur, M. 1996, ApJ, 457, 415
ESA 1997, VizieR Online Data Catalog, 1239, 0
Fedele, D., Wittkowski, M., Paresce, F., et al. 2005, A&A, 431, 1019
Herpin, F., Baudry, A., Thum, C., Morris, D., & Wiesemeyer, H. 2003, in SF2A-2003: Semaine de l'Astrophysique Francaise, 523
Herpin, F., Baudry, A., Thum, C., Morris, D., & Wiesemeyer, H. 2006, A&A, 450, 667
Humphreys, E. M. L., Gray, M. D., Yates, J. A., et al. 1996, MNRAS, 282, 1359
Humphreys, E. M. L., Gray, M. D., Yates, J. A., et al. 2002, A&A, 386, 256
Ireland, M. J., & Scholz, M. 2006, MNRAS, 367, 1585
Ireland, M. J., Tuthill, P. G., Bedding, T. R., Robertson, J. G., & Jacob, A. P. 2004, MNRAS, 350, 365
Justtanont, K., de Jong, T., Tielens, A. G. G. M., Feuchtgruber, H., & Waters, L. B. F. M. 2004, A&A, 417, 625
Karovska, M., Schlegel, E., Hack, W., Raymond, J. C., & Wood, B. E. 2005, ApJ, 623, L137
Kemball, A. J., & Diamond, P. J. 1997, ApJ, 481, L111
McIntosh, G. C. 2006, ApJ, 649, 406
Mennesson, B., Perrin, G., Chagnon, G., et al. 2002, ApJ, 579, 446
Menut, J.-L., Chesneau, O., Lopez, B., et al. 2004, in New Frontiers in Stellar Interferometry, ed. W. A. Traub (Bellingham, WA: The International Society for Optical Engineering), Proc. SPIE, 5491, 1733
Millan-Gabet, R., Pedretti, E., Monnier, J. D., et al. 2005, ApJ, 620, 961
Monnier, J. D., Millan-Gabet, R., Tuthill, P. G., et al. 2004, ApJ, 605, 436
Nedoluha, G. E., & Watson, W. D. 1990, ApJ, 354, 660
Nedoluha, G. E., & Watson, W. D. 1994, ApJ, 423, 394
Ohnaka, K., Bergeat, J., Driebe, T., et al. 2005, A&A, 429, 1057
Perrin, G., Ridgway, S. T., Mennesson, B., et al. 2004, A&A, 426, 279
Ragland, S., Traub, W. A., Berger, J.-P., et al. 2006, ApJ, 652, 650
Reid, M. J., & Menten, K. M. 1997, ApJ, 476, 327
Reid, M. J., & Moran, J. M. 1981, ARA&A, 19, 231
Schuller, P., Salomé, P., Perrin, G., et al. 2004, A&A, 418, 151
Suh, K.-W. 2004, ApJ, 615, 485
Tatebe, K., Chandler, A. A., Hale, D. D. S., & Townes, C. H. 2006, ApJ, 652, 666
Vlemmings, W. H. T., Diamond, P. J., & Imai, H. 2006, Nature, 440, 58
Vlemmings, W. H. T., van Langevelde, H. J., & Diamond, P. J. 2005, A&A, 434, 1029
Weiner, J. 2004, ApJ, 611, L37
Weiner, J., Hale, D. D. S., & Townes, C. H. 2003a, ApJ, 589, 976
Weiner, J., Hale, D. D. S., & Townes, C. H. 2003b, ApJ, 588, 1064
Woodruff, H. C., Eberhardt, M., Driebe, T., et al. 2004, A&A, 421, 703